Dispersion in Silica *Microbubble Resonators*

NICOLAS RIESEN,[1,*] WEN QI ZHANG,[1,2] TANYA M. MONRO[1,2]

[1]*Institute for Photonics and Advanced Sensing (IPAS) and School of Physical Sciences, The University of Adelaide, SA 5005, Adelaide, Australia*
[2]*University of South Australia, SA 5001, Adelaide, Australia*
**Corresponding author: nicolas.riesen@adelaide.edu.au*

We explore the scope for engineering dispersion in whispering gallery mode silica microbubbles for nonlinear applications such as optical frequency comb generation. In particular, the zero dispersion wavelength is shown to be highly tunable by changing the thickness of the shell. Using a small diameter and small wall thickness, dispersion equalization within the visible is predicted. This opens up the possibility of realizing visible frequency combs for a range of different applications.

OCIS codes: *(140.3945) Microcavities; (190.4360) Nonlinear optics, devices; (190.4380) Nonlinear optics, four-wave mixing; (230.5750) Resonators.*

Over the past few decades whispering gallery mode (WGM) resonators have found increasing use in biological and chemical sensing applications [1-5]. Whispering gallery resonators typically have small mode volumes V and high Q-factors which allow for high energy densities and long photon storage lifetimes [6]. One specific class of whispering gallery resonators that has gained considerable interest in recent years are microbubble resonators [7-17]. Microbubble (or microshell) resonators are thin-walled spherical shells that can support whispering gallery modes with evanescent fields inside and outside of the resonator [10]. They typically have wall thicknesses ranging from ~0.4 - 8 μm [12, 18], and Q-factors up to 10^7 [7, 19, 20]. When the walls have a thickness of the order of the wavelength of light the evanescent fields can extend far outside the cavity wall resulting in a highly sensitive resonator ideal for various sensing applications [6].

Some of the applications of microbubble resonators include refractive index sensing [10, 14, 18, 19], optomechanical measurement of mass and acceleration [10], temperature sensing [10, 11] and pressure sensing [13, 19]. Microbubbles are also of particular interest for biochemical sensing because they allow the samples to be placed inside the resonator, avoiding disturbance of the coupling mechanism with e.g. a tapered optical fiber. More recently microbubbles have also been used for optical frequency comb generation through hyperparametric excitation of the WGMs [20].

Optical frequency combs have found use in a range of applications relating to metrology, spectroscopy and sensing [21-23]. The basic process by which frequency comb generation occurs in microresonators is four-wave mixing (FWM) which propagates along the resonances provided that there is zero dispersion [21, 24-26]. Zero dispersion ensures that the WGM resonance frequencies (i.e. the frequency comb teeth) are equally spaced. This is necessary for maintaining energy conservation as the FWM process cascades along the resonances.

The extremely small mode volumes V possible in microbubbles is particularly beneficial for frequency comb generation as it enhances the nonlinear interaction due to the increased energy density. Moreover, the extra degree of freedom provided by the thickness of the microbubble walls, when compared with solid spheres, allows for much more effective tailoring of the dispersion. The key requirements for frequency comb generation to occur in microresonators are zero dispersion and a high Q^2/V value [20, 21, 27]. In this letter we consider both these facets as functions of diameter and shell thickness for silica microbubbles.

The total dispersion of a microbubble resonator, which consists of both material and geometric components, can be determined by first solving the resonance wavelengths of the transverse electric (TE) or transverse magnetic (TM) whispering gallery modes.

The TE and TM WGM resonance wavelengths of a microbubble can be solved using the general model of a microsphere with a high-index coating described in [28, 29]. For the case of microbubbles the inner sphere is assumed to have an index of one, whilst the medium surrounding the resonator could be varied as required. By incorporating the wavelength-dependence of the refractive indices in the calculation using the relevant Sellmeier equations, the exact resonance wavelengths can be solved. The Sellmeier equation for silica (i.e. fused/amorphous SiO_2) is given by [30]. The resonances are categorized by two quantum numbers q and l. The radial mode number q determines the number of nodes of the WGM in the radial direction, whereas the azimuthal mode number l determines the number of nodes in the azimuthal direction. In this letter only the first-order modes (q = 1) are considered which are the smallest wavenumber k solutions for each azimuthal mode number l. To ensure correct identification of the first-order mode for a given azimuthal mode number l, the script implemented solves the characteristic equation given in [28, 29], for multiple initial wavelength guesses over an appropriate wavelength range. The solutions are then ordered, with the largest wavelength value corresponding to the first-order q = 1 mode.

Once the first-order resonances are determined for a range of l, the total cavity dispersion is then given by the change in free-spectral range (FSR) over the resonances, $\Delta(\Delta\nu_l)$, where ν_l are the discrete resonance frequencies.

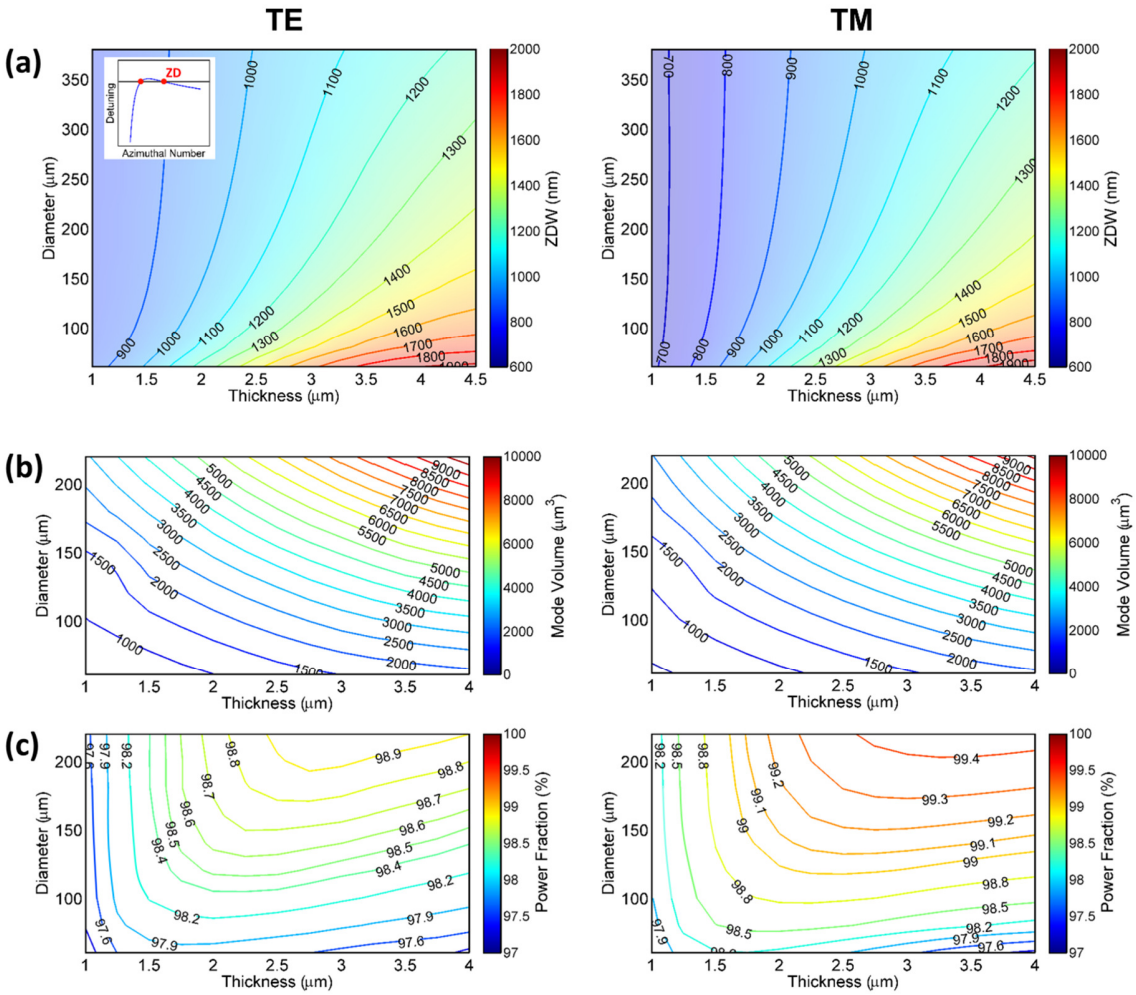

Fig. 1. (a) The zero dispersion wavelength for the first-order TE and TM modes of silica microbubbles as a function of diameter and wall thickness. Inset of (a) shows a typical detuning curve (blue) with zero crossings (red points) of which only the shortest wavelength solution is considered. The (b) mode volume and (c) power fraction in the shell, across the relevant ZDW space.

The zero dispersion wavelength for the microbubble of given thickness and diameter is then determined from the resonance frequency, corresponding to azimuthal mode l, nearest to the zero crossing of $\Delta(\Delta\nu_l)$. An example of a detuning curve is shown in the inset of Fig. 1 (a). For microbubble resonators there are typically two or more ZDW solutions of which the shortest wavelength solution is considered here. The presence of multiple ZDWs allows for relatively flat dispersion to be realized over a large wavelength range, a feature which is usually not possible for microsphere resonators [20, 27]. Flat dispersion is critical for achieving broadband frequency comb generation [21, 22].

The ZDWs of silica microbubbles as a function of diameter and shell thickness, are shown in Fig. 1 for the TE and TM modes. The ZDW is found to change dramatically as the diameter (40-380 μm) and wall thickness (1-4.5 μm) is varied. As shown in Fig. 1 (a), the ZDW varies from ~600 nm at small diameters and small wall thicknesses to ~1900 nm at large wall thicknesses. The results are in agreement with specific cases previously modelled by Li *et al* [20]. The results demonstrate over one octave tuning of the ZDW, for the current parameter space, by way of altering the geometry. This ZDW range is considerably larger than that possible with silica microsphere resonators [27]. The broader ZDW range for the microbubbles arises because of the additional degree of freedom provided by the shell thickness for adjusting the geometric component of dispersion by altering the degree of light confinement.

Also note that as the thickness and diameter increase, the ZDW naturally converges to that of bulk material (λ_{ZD} = 1.27 μm) since the geometric dispersion contribution diminishes. The ZDW (nm) can be approximated, over the parameter space considered, using a third-order polynomial fit of the form,

$$\lambda_{ZD}(t,d) = c_0 + c_1 t + c_2 d + c_3 t d + c_4 d^2 + c_5 t d^2 + c_6 d^3 \quad (1)$$

where c_i are the coefficients, d (μm) is the microbubble diameter and t (μm) is the wall thickness.

Table 1. Zero dispersion wavelength polynomial fit.

Coefficients	TE	TM
c_0	754	440
c_1	399	466
c_2	-3.89	-2.51
c_3	-1.47	-1.80
c_4	2.23×10^{-2}	1.91×10^{-2}
c_5	2×10^{-3}	2.63×10^{-3}
c_6	-3.34×10^{-5}	-3.17×10^{-5}

This particular third-order polynomial was used as it provides a good approximation of the sharp rise in ZDW occurring for small diameters and large wall thickness. The coefficients for the polynomial fit for the TE and TM modes ($R^2 \sim 0.99$) are given in Table 1.

At this point it is interesting to note that the ZDWs of the TE modes are in general higher than those of the TM modes. This differs from microspheres for which the ZDW is largely independent of polarization [27]. Indeed, as the wall thickness increases, and the resonator geometry approaches that of a microsphere, the discrepancy in ZDWs for the two polarizations diminishes. The polarization dependence is due to the silica-air interfaces. The high index contrast results in large discontinuities in the perpendicular electric fields due to the relevant boundary conditions. The effective index of the TM modes is therefore more sensitive to the wall thickness than the TE modes, resulting in greater geometric dispersion for the TM modes. This accounts for the discrepancy in ZDWs for the two polarizations. For the same reason the mode volume of the TM modes is marginally smaller as shown in Fig. 1 (b). This is true in the present case where the wall thicknesses are greater than the operating wavelength.

The mode volumes were determined from the cross-sectional electric field distributions of the WGMs which were obtained using a finite-element method (FEM) simulation in which axial symmetry is used to reduce the 3D problem to 2D [31]. As an example, the normalized radial electric field distributions (logarithmic scale) for the first-order modes of a silica microbubble are shown in Fig. 2, as the shell thickness is varied (1-4 μm) for a fixed diameter (120 μm). Note that as the shell thickness varies the operating wavelength, assumed to be the zero dispersion wavelength, also varies. The figure demonstrates how the field distribution (and thus mode volume) varies dramatically as the shell thickness is changed. In general, reducing the shell thickness reduces the mode volume, allowing for significant enhancements in the nonlinear interaction efficiency.

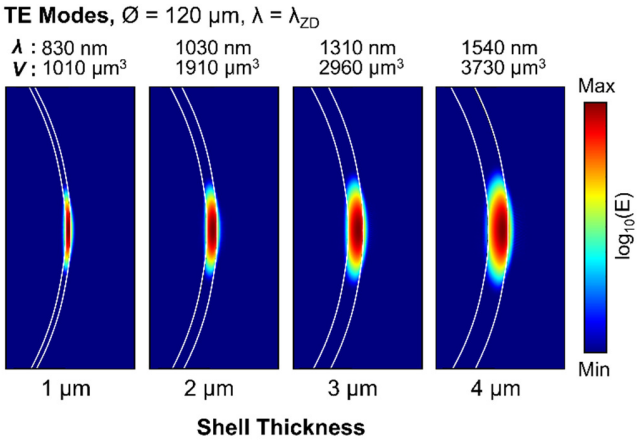

Fig. 2. The normalized radial electric field distributions ($\log_{10}(E)$) for a 120 μm diameter silica microbubble as the thickness ranges from 1-4 μm. The azimuthal mode number ranges from l = 639 to 342.

The mode volume V, as well as the power fraction inside the shell P, were quantified as follows,

$$V = \frac{\int \varepsilon \mid E \mid^2 dV}{\max\left(\varepsilon \mid E \mid^2\right)}, \quad P = \frac{\int_{wall} \varepsilon \mid E \mid^2 dV}{\int \varepsilon \mid E \mid^2 dV} \qquad (2)$$

where E is the electric field and ε is the permittivity of silica. The mode volume was integrated over a region slightly larger than the resonator that was scaled with the diameter of the resonator. As shown in Fig. 1 (b) the mode volume for silica microbubbles varies from 100s μm³ to 10,000 μm³ over the entire parameter space modelled. As expected the mode volume in general increases with increasing diameter and wall thickness. Also, for the first-order fundamental modes modelled the fraction of power in the shell Eq. (2), is close to 100% as shown in Fig. 1 (c), whereas for higher-order modes or subwavelength wall thicknesses a large proportion of the light resides outside the shell [18].

As mentioned the mode volume can be decreased significantly up to a certain point, by decreasing the wall thickness, although a trade-off with the Q-factor would need to be considered for very thin walls to ensure optimal performance [6]. High Q-factor WGMs can only be supported in microbubbles with wall thicknesses comparable to or greater than the wavelength of light [6, 14]. Yang *et al.*, also suggest that TE modes tend to have higher Q-factors compared with TM modes, and this is especially true as the thickness of the shell decreases [14]. Note that for the silica microbubbles considered in this letter, the Q-factor is material absorption-limited, with geometric losses being negligible [14]. The Q-factor due to material absorption can be approximated as,

$$Q_{mat} \approx \frac{2\pi n_{eff}}{P\,\alpha\lambda} \qquad (3)$$

where n_{eff} is the effective mode index, P is the power fraction of light confined to the shell, $\alpha = \alpha(\lambda)$ is the bulk material attenuation (dB/m) and λ is the free-space operating wavelength. The material absorption-limited Q-factor of the silica microbubbles considered is shown in Fig. 3 (a) at the zero dispersion wavelength (i.e. $\lambda = \lambda_{ZD}$). The Q-factor varies from approximately 10^9 to 10^{10} over the parameter space. This Q-factor represents an upper theoretical limit in vacuum assuming zero absorption in the surrounding medium and negligible surface scattering.

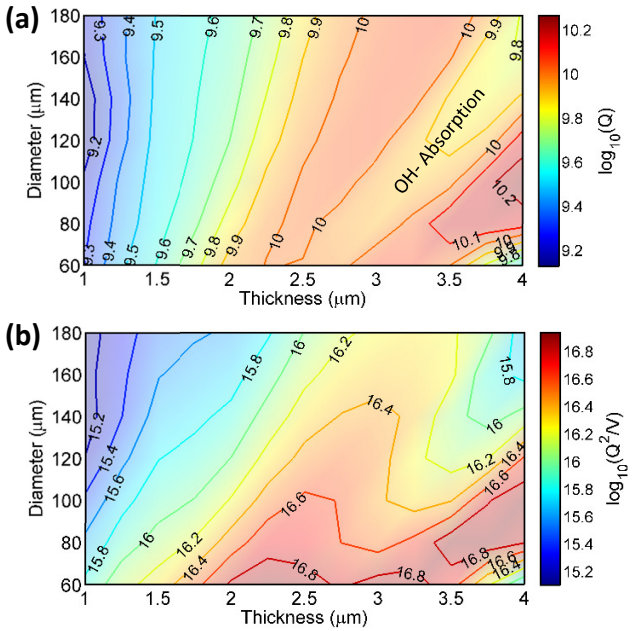

Fig. 3. (a) The material absorption Q-factor component, Q_{mat}, at the zero dispersion wavelength ($\lambda = \lambda_{ZD}$) for the TM first-order modes of silica microbubbles as a function of diameter and wall thickness. (b) The corresponding Q^2/V values. Material absorption interpolated from [32].

The Q-factor is maximal eitherside of the OH^- absorption peak (1380 nm) of silica, corresponding with larger diameters and wall thicknesses. On the other hand, the nonlinear figure of merit Q^2/V [μm^{-3}] shown in Fig. 3 (b), is optimized for smaller diameters since the mode volume

rapidly increases at larger diameters. Therefore smaller diameters generally lead to higher Q^2/V values and hence a reduced power threshold for comb generation. The Q^2/V values range from a minimum of $\sim 10^{15}$ μm^{-3} at $\lambda_{ZD} = 600$ nm to a maximum of $\sim 10^{17}$ μm^{-3} at $\lambda_{ZD} = 1600$ nm. The relatively high Q^2/V values predicted even for shorter ZDWs corresponding to smaller wall thicknesses, suggests that relatively low power thresholds for comb generation can still be expected even in the visible.

We also note that the ZDW of silica microbubbles is likely to extend further into the visible for microbubbles with diameters even smaller than those considered here. Provided that the wall thickness is larger than the wavelength of light, high Q-factors are still expected for smaller microbubbles [14], implying that frequency comb generation in the visible is likely to be possible. As suggested, this is especially true given that the small mode volumes of microbubble resonators will enhance the nonlinear interaction efficiency as quantified by the figure of merit (Q^2/V). The short operating wavelength would also contribute to the enhanced mode confinement.

It is also found that when the silica microbubble has a surrounding medium of water the ZDW changes only marginally, provided that the wall thickness is not subwavelength. Therefore dispersion equalization could still be realized in the visible for silica microbubbles submerged in water. Given that the low-loss wavelength window of water is in the visible [33], the possibility exists for realizing the high absorption-limited Q-factors [34] necessary for comb generation in aqueous solution for applications such as biosensing.

In conclusion, this letter has explored the opportunities existing for engineering dispersion in silica microbubble resonators by varying the diameter and shell thickness. It is shown that dispersion equalization within the visible is possible for small microbubbles (<100 μm) with thin walls (~1 μm). The realization of dispersion equalization within the visible, in addition to the small mode volumes possible for thin-walled structures, could provide novel opportunities in nonlinear optics for this emerging class of resonators especially in terms of visible frequency comb generation.

Funding. Australian Research Council (ARC) (FL130100044).

Acknowledgment. The authors thank S. A. Vahid and A. François for insightful discussions.

References

1. A. Matsko, A. Savchenkov, D. Strekalov, V. Ilchenko, and L. Maleki, IPN Progress Report **42**, 162 (2005).
2. F. Vollmer and S. Arnold, Nat. Methods **5**, 591 (2008).
3. F. Vollmer, S. Arnold, and D. Keng, Proc. Natl. Acad. Sci. USA **105**, 20701 (2008).
4. A. Chiasera, Y. Dumeige, P. Feron, M. Ferrari, Y. Jestin, G. N. Conti, S. Pelli, S. Soria, and G. C. Righini, Laser Phot. Rev. **4**, 457 (2010).
5. M. D. Baaske, M. R. Foreman, and F. Vollmer, Nat. Nanotech. **9**, 933 (2014).
6. Y. Yang, J. Ward, and S. N. Chormaic, in *SPIE LASE*, (International Society for Optics and Photonics, 2014), p. 89600I.
7. S. Berneschi, D. Farnesi, F. Cosi, G. N. Conti, S. Pelli, G. Righini, and S. Soria, Opt. Lett. **36**, 3521 (2011).
8. M. Sumetsky, Y. Dulashko, and R. Windeler, Opt. Lett. **35**, 1866 (2010).
9. P. Wang, J. Ward, Y. Yang, X. Feng, G. Brambilla, G. Farrell, and S. N. Chormaic, Appl. Phys. Lett. **106**, 061101 (2015).
10. J. Ward, Y. Yang, R. Madugani, and S. N. Chormaic, in *Photonics Conference (IPC), 2013* (IEEE, 2013), p. 452.
11. J. M. Ward, Y. Yang, and S. N. Chormaic, in *SPIE LASE*, (International Society for Optics and Photonics, 2014), p.89601W.
12. A. Watkins, J. Ward, Y. Wu, and S. N. Chormaic, Opt. Lett. **36**, 2113 (2011).
13. Y. Yang, S. Saurabh, J. Ward, and S. N. Chormaic, Opt. Lett. **40**, 1834 (2015).
14. Y. Yang, J. Ward, and S. N. Chormaic, Opt. Express **22**, 6881 (2014).
15. Z. Yu, T. Liu, J. Jiang, K. Liu, W. Chen, X. Zhang, X. Lin, and W. Liu, in *SPIE/COS Photonics Asia 2014* (International Society for Optics and Photonics, 2014), p. 92740L.
16. N. Lin, L. Jiang, S. Wang, Q. Chen, H. Xiao, Y. Lu, and H. Tsai, Appl. Opt. **50**, 5465 (2011).
17. H. Li, Y. Guo, Y. Sun, K. Reddy, and X. Fan, Opt. Express **18**, 25081 (2010).
18. W. Lee, Y. Sun, H. Li, K. Reddy, M. Sumetsky, and X. Fan, Appl. Phys. Lett. **99**, 091102 (2011).
19. R. Henze, T. Seifert, J. Ward, and O. Benson, Opt. Lett. **36**, 4536 (2011).
20. M. Li, X. Wu, L. Liu, and L. Xu, Opt. Express **21**, 16908 (2013).
21. T. J. Kippenberg, R. Holzwarth, and S. Diddams, Science **332**, 555 (2011).
22. C. Y. Wang, T. Herr, P. Del'Haye, A. Schliesser, J. Hofer, R. Holzwarth, T. W. Hänsch, N. Picqué, and T. J. Kippenberg, Nat. Comm. **4**, 1345 (2013).
23. J. Ye, *Femtosecond optical frequency comb: principle, operation and applications* (Springer, 2005).
24. I. H. Agha, Y. Okawachi, M. A. Foster, J. E. Sharping, and A. L. Gaeta, Phys. Rev. A **76**, 043837 (2007).
25. P. Del'Haye, A. Schliesser, O. Arcizet, T. Wilken, R. Holzwarth, and T. Kippenberg, Nature **450**, 1214 (2007).
26. D. Ristić, M. Mazzola, A. Chiappini, A. Rasoloniaina, P. Féron, R. Ramponi, G. C. Righini, G. Cibiel, M. Ivanda, and M. Ferrari, Opt. Lett. **39**, 5173 (2014).
27. N. Riesen, S. Afshar V, A. François, and T. M. Monro, Opt. Express **23**, 14784 (2015).
28. I. Teraoka and S. Arnold, JOSA B **24**, 653 (2007).
29. I. Teraoka and S. Arnold, JOSA B **23**, 1434-1441 (2006).
30. I. H. Malitson, JOSA **55**, 1205 (1965).
31. M. Oxborrow, IEEE Trans. Microw. Theory Techn. **55**, 1209 (2007).
32. Olson Technology, "A brief history of optical fiber," http://www.olson-technology.com/mr_fiber/fiber-history.htm.
33. D. J. Segelstein, "The complex refractive index of water," (PhD Thesis, University of Missouri--Kansas City, 2011).
34. A. Armani, D. Armani, B. Min, K. Vahala, and S. Spillane, Appl. Phys. Lett. **87**, 151118 (2005).